

Spatial Variability of Barrow-Area Shore-Fast Sea Ice and Its Relationships to Passive Microwave Emissivity

James A. Maslanik, Matthew Sturm, Maria Belmonte Rivas, Albin J. Gasiewski, *Fellow, IEEE*, John F. Heinrichs, *Member, IEEE*, Ute C. Herzfeld, Jon Holmgren, Marian Klein, *Member, IEEE*, Thorsten Markus, *Member, IEEE*, Donald K. Perovich, John G. Sonntag, Julienne C. Stroeve, and Ken Tape

Abstract—Aircraft-acquired passive microwave data, laser radar height observations, RADARSAT synthetic aperture radar imagery, and *in situ* measurements obtained during the AMSR-Ice03 experiment are used to investigate relationships between microwave emission and ice characteristics over several space scales. The data fusion allows delineation of the shore-fast ice and pack ice in the Barrow area, AK, into several ice classes. Results show good agreement between observed and Polarimetric Scanning Radiometer (PSR)-derived snow depths over relatively smooth ice, with larger differences over ridged and rubbled ice. The PSR results are consistent with the effects on snow depth of the spatial distribution and nature of ice roughness, ridging, and other factors such as ice age. Apparent relationships exist between ice roughness and the degree of depolarization of emission at 10, 19, and 37 GHz. This depolarization would yield overestimates of total ice concentration using polarization-based algorithms, with indications of this seen when the NT-2 algorithm is applied to the PSR data. Other characteristics of the microwave data, such as effects of grounding of sea ice and large contrast between sea ice and adjacent land, are also apparent in the PSR data. Overall, the results further demonstrate the importance of macroscale ice roughness conditions such as ridging and rubbing on snow depth and microwave emissivity.

Index Terms—Passive microwave, roughness, sea ice, shore-fast ice, snow depth.

Manuscript received November 17, 2005; revised April 25, 2006. This work was supported by the National Aeronautics and Space Administration under the AMSR Validation Program and Grant NNG04GH68G.

J. A. Maslanik and M. Belmonte Rivas are with the Colorado Center for Astrodynamics Research, University of Colorado, Boulder, CO 80309 USA (e-mail: james.maslanik@colorado.edu).

M. Sturm and J. Holmgren are with the U.S. Army Cold Regions Research and Engineering Laboratory-Alaska, Fairbanks, AK 99775 USA.

A. J. Gasiewski is with the Department of Electrical and Computer Engineering, University of Colorado, Boulder, CO 80309 USA.

J. F. Heinrichs is with the Ft. Hays State University, Hays, KS 67601 USA.

U. C. Herzfeld and J. C. Stroeve are with the Cooperative Institute for Research in Environmental Sciences, University of Colorado, Boulder, CO 80309 USA.

M. Klein is with the NOAA Environmental Technology Laboratory, Boulder, CO 80305 USA.

T. Markus is with the NASA Goddard Space Flight Center, Greenbelt, MD 20771 USA.

D. K. Perovich is with the U.S. Army Cold Regions Research and Engineering Laboratory, Hanover, NH 03755 USA.

J. G. Sonntag is with the NASA Wallops Flight Facility, Goddard Space Flight Center, Greenbelt, MD 20771 USA.

K. Tape is with the Geophysical Institute, University of Alaska Fairbanks, Fairbanks, AK 99775 USA.

Digital Object Identifier 10.1109/TGRS.2006.879557

I. INTRODUCTION

THE SEA-ICE cover is typically highly variable over short distances (e.g., [1] and [2]), particularly in terms of surface roughness. Numerous studies have pointed out the importance of ice formation, deformation, and melt processes on this variability as well as overall surface roughness conditions [3]–[5]. However, the scales of surface variability are not well known [6], and there is relatively little information available regarding how the aggregate effects of such spatial variability influence brightness temperatures observed from satellites [7]. Eppler *et al.* [3] note that emissivities of ice ridges vary as a function of ice type and aging processes. Farmer *et al.* [8] specifically examined the microwave signatures of ridges within the perennial ice pack and found a wide range of brightness temperatures. They attributed this variability to the mixtures of ice within ridges (i.e., ridged first-year ice between multiyear floes, etc.) and to processes associated with aging of ridges such as ice metamorphism and snow accumulation. Lohanick [9] describes the ability of snow cover to mask underlying ice features. These and other studies provide excellent examples of the effects of ice and snow characteristics on microwave emissivity, but many of these pioneering investigations were limited by the availability of only a single channel of aircraft-acquired microwave imagery (33.4 GHz, single polarization).

The AMSR-Ice03 validation program [2], [10] carried out on shore-fast ice near Barrow, AK, during March 4–19, 2003, provides an opportunity to extend such work through the use of multichannel microwave data in concert with other data and *in situ* observations. Our objective is to investigate relationships between sea-ice macroscale (meter to tens of meters) surface roughness and brightness temperatures. Specifically, we wish to learn more about how variations in ice conditions associated with roughness and geometric complexity affect passive microwave-derived sea-ice products and, in particular, products generated by the Advanced Microwave Scanning Radiometer for the Earth Observing System (AMSR-E) passive microwave sensor on the EOS Aqua platform. Our approach is to combine the detailed *in situ* measurements described by Sturm *et al.* [2] with aircraft and satellite data to extrapolate point measurements to the larger scale, spanning the domain of the Barrow, shore-fast ice and adjacent pack-ice study area (Fig. 1). As is documented by Sturm *et al.* [2], the *in situ* transects spanned a range of first-year ice conditions over shore-fast sea ice, from smooth ice to heavily ridged and rubbled ice.

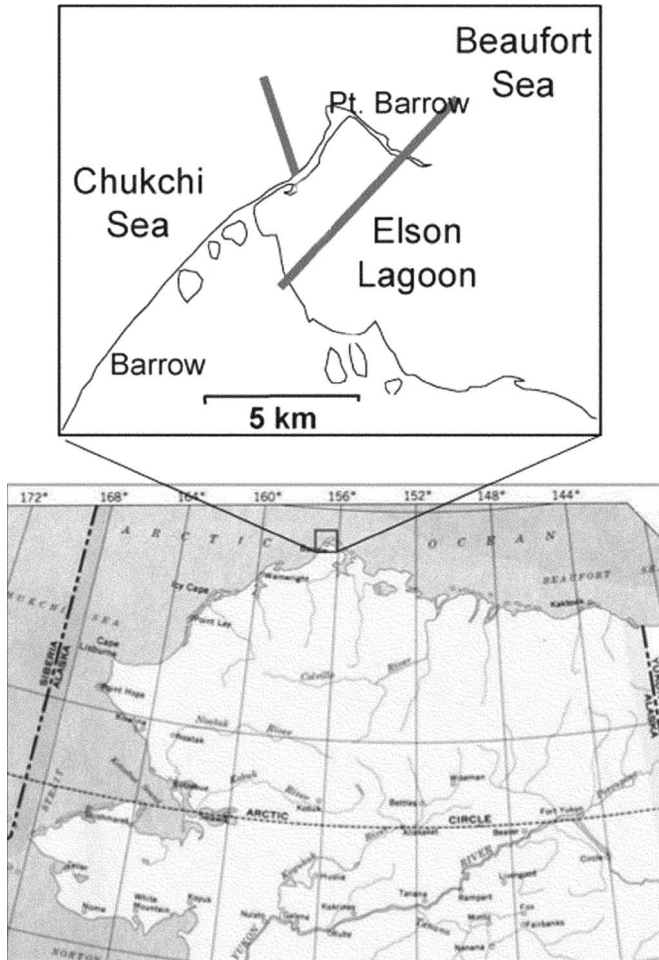


Fig. 1. Study area and location of measurement transects.

A key guiding principle for the *in situ* component of the AMSR-Ice03 experiment was that data be collected by a combination of means in a manner that would allow us to bridge spatial scales from point measurements through AMSR-sized pixel dimensions. Data acquired by the NASA P-3 aircraft provide this link. With this in mind, the AMSR-Ice03 experiment was designed such that the NASA P-3 would acquire Polarimetric Scanning Radiometer (PSR) data at a 55° incidence angle [11] from low-altitude (approximately 150 m) passes over specified field transect locations to provide maximum spatial resolution coincident with the surface measurements. In addition to these low-level overpasses, the P-3 flew a grid pattern at higher elevation (about 1400 m) to provide data at scales of tens to hundreds of meters—intermediate between the point measurements and kilometer-scale satellite imagery.

II. DATA

Given that microwave data are affected by roughness at different spatial scales (e.g., [12]), the sampling strategy developed for AMSR-Ice03 provided information on surface conditions at microwave wavelength scales through scales of hundreds of meters typically associated with large-scale ice kinematics. The analysis and results presented here make use of *in situ* data, PSR imagery, and Airborne Terrain Mapper (ATM laser) [13], [14] surface heights acquired during the

1400-m flight tracks over the Barrow area [15] and PSR data collected in non-scanning mode during the 150-m flight tracks over the field transects, along with satellite imagery in the form of RADARSAT synthetic aperture radar (SAR) ScanSAR imagery. The PSR measured microwave brightness temperatures ($T_{B,ij}$, where i is frequency and j is polarization) at four channels with vertical and horizontal polarizations: $T_{B,10V,H}$, $T_{B,19V,H}$, $T_{B,37V,H}$, and $T_{B,89V,H}$ (see [11] for details of the PSR instrument and P-3 operations). The PSR and SAR data were mapped to a Universal Transverse Mercator projection and gridded at two resolutions: 100-m pixel size for PSR and SAR gridding over the larger area and 25-m pixel size to retain the full resolution of the PSR data acquired during the 120-m overpasses over the field transects. We make use of $T_{B,10V,H}$, $T_{B,19V,H}$, and $T_{B,37V,H}$ here. PSR data at 89 GHz were not used in quantitative analysis due to uncertainties in calibration. Aerial photographs acquired by the P-3 and a single-engine aircraft, along with low-level digital photographs and skin temperatures obtained by Aerosonde unpiloted aerial vehicles [16], [17], provide additional moderate- to high-resolution information offering fine spatial detail and context information critical for interpreting relationships between ice conditions in an overall setting (e.g., [18]).

III. RESULTS

A. Ice Regime Classification

Sturm *et al.* [2] describe the ice conditions encountered in the Barrow study area. As they note, the study site includes ice with a range of roughness conditions and general morphology. Since these conditions are particularly relevant to the analysis here, we provide additional examples of ice characteristics and then use this knowledge to extend the general classification of ice according to general roughness categories.

Fig. 2 illustrates the typical ice conditions found in various locations along the measurement transects on the shore-fast ice. As the photographs suggest, the Chukchi transect covered the smoothest area of ice observed visually. This transect extended from near the shoreline north-northwest to the point where extensive ridging and rubbling began. Based on visual observations and aerial photographs, the surface along the Elson Lagoon transect was rougher, with larger snow drifts [2], [19], but still relatively uniform in appearance. The section of transect in the Beaufort Sea spanned a mixture of heavily rubbled ice and large (approximately 3–5 m) ridges, with interspersed floes and/or refrozen areas that were smooth and wind scoured.

In addition to illustrating ice conditions along the transects, Fig. 2 provides a general key to the interpretation of the SAR image, PSR images, and other data discussed below. Based on *in situ* ice reconnaissance, aerial photographs, and an understanding of empirical relationships between ice conditions and SAR backscatter, passive microwave emissivity, and ATM roughness, the study area was mapped into a set of ice regimes that capture the main categories of complexity of the ice cover as defined by roughness and variability of the surface. This provides one means of extrapolating the detailed measurements obtained along the transects to the entire study area, thus helping bridge the gap in spatial scales between point observations and the aircraft-acquired PSR data.

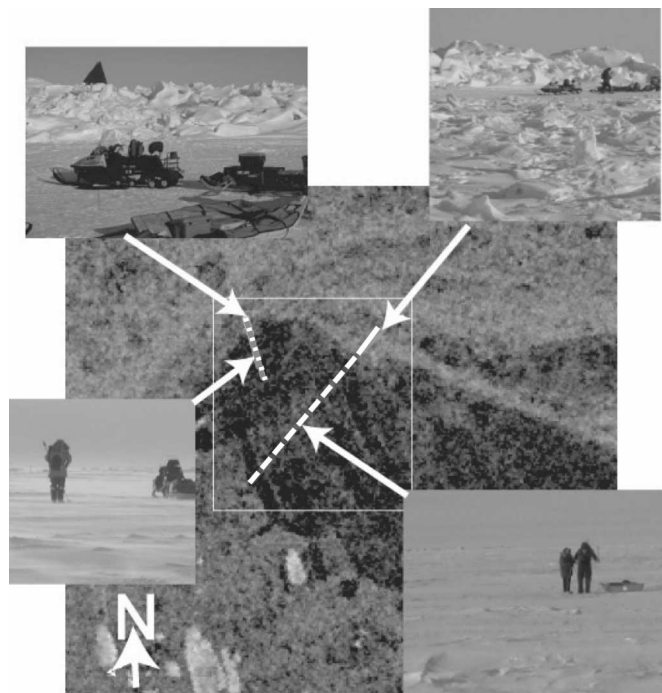


Fig. 2. Examples of ice conditions (photo insets) at different locations along the primary field transects [indicated by the dashed white line (Elson transect), dotted white line (Chukchi transect), and solid white line (Beaufort transect)]. One of the tetrahedron targets described by Sturm *et al.* [2] is visible in the upper left photo, marking the northernmost end of the Chukchi transect.

The false-color composite of SAR, $T_{B,19V}$, and $T_{B,37V}$ in the top panel in Fig. 3 can be interpreted as follows: reddish-yellow areas correspond to heavily ridged and rubbled ice that forms along the seaward edge of the Chukchi shore-fast ice as well as to the east and north of Point Barrow. In both locations, a portion of the ice typically becomes grounded to the sea floor (the “*stamukhi*” zone). The striated banding east and northeast of Point Barrow is typical of the area in most years and reflects the general easterly motion of the pack ice that produces large shear and pressure zones running generally east and west. The reddish-yellow tones in the top panel in Fig. 3 indicate high SAR backscatter along with low emissivity at $T_{B,19V}$ and $T_{B,37V}$. (Note that surface and ice temperatures were relatively uniform over the study area; thus, differences in observed T_B can be attributed primarily to differences in emissivity.) In contrast, greenish-white areas are associated with relatively smooth portions of the ice cover, with low backscatter and similar $T_{B,19V}$ and $T_{B,37V}$ values. The greenish-blue locations are areas that have intermediate backscatter values and where $T_{B,37V}$ is substantially less than $T_{B,19V}$. Within Elson Lagoon, the green areas correspond to areas of moderately to lightly rubbled ice that have deeper snowpack than elsewhere within the lagoon, as described by Sturm *et al.* [2] and below. The pack-ice areas show variable patterns, with generally high backscatter overall (associated with rougher ice and possibly recently formed frost flowers on new ice) but with some individual floes apparent based on their lower backscatter. These floes are likely to be older first-year ice floes within a younger rougher matrix of first-year ice. No multiyear ice was observed in the study area. These

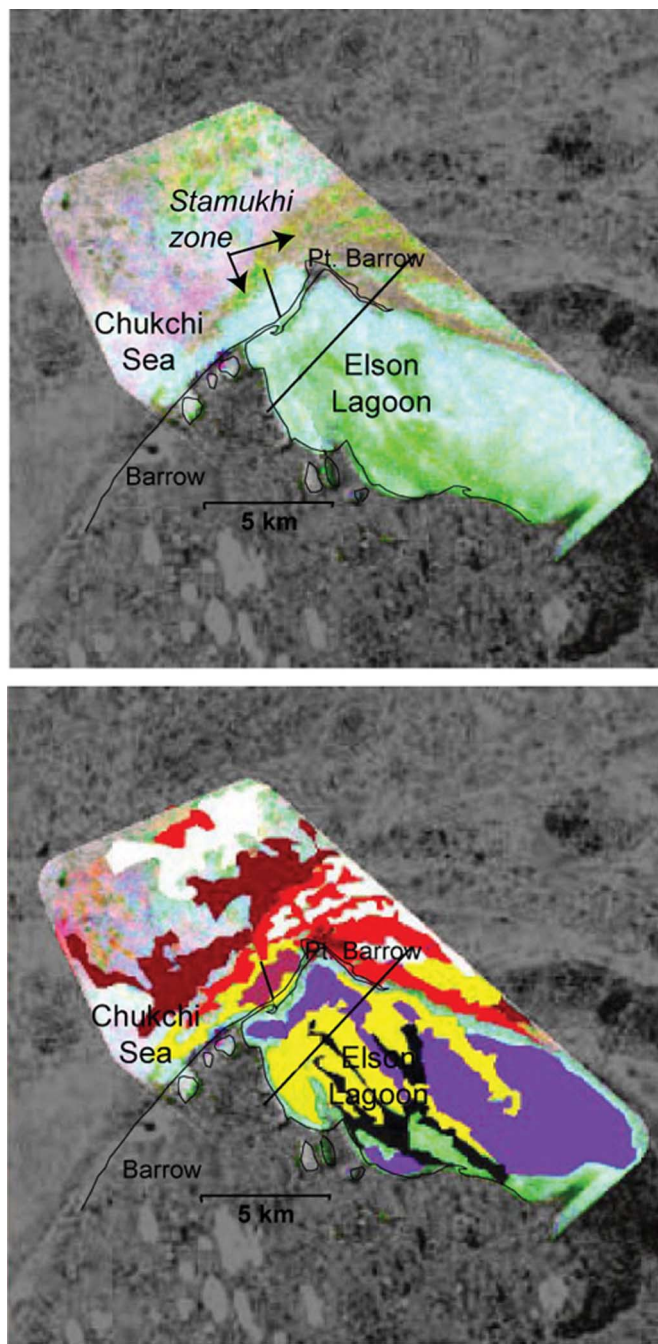


Fig. 3. (Top) False-color composite of SAR data (red image channel), PSR $T_{B,19V}$ (green channel), and PSR $T_{B,37V}$ (blue channel). A manual classification of the same three channels is shown in the bottom panel. The gray areas show SAR backscatter for areas without corresponding PSR coverage. The classes are ridged ice (red), heavily rubbled ice (white), moderately rubbled ice (black), lightly rubbled ice (yellow), moderately smooth ice (blue), and smooth ice (purple). The general *stamukhi* zone area is indicated in the top panel. The locations of the field transects are shown by the black lines, as in Figs. 1 and 2.

general interpretations of ice conditions are consistent with ATM-derived ice roughness observations (Fig. 4) [15], which confirm the greater height variations in ridged areas and the presence of relatively smooth ice in the nearshore portion of the Chukchi transect.

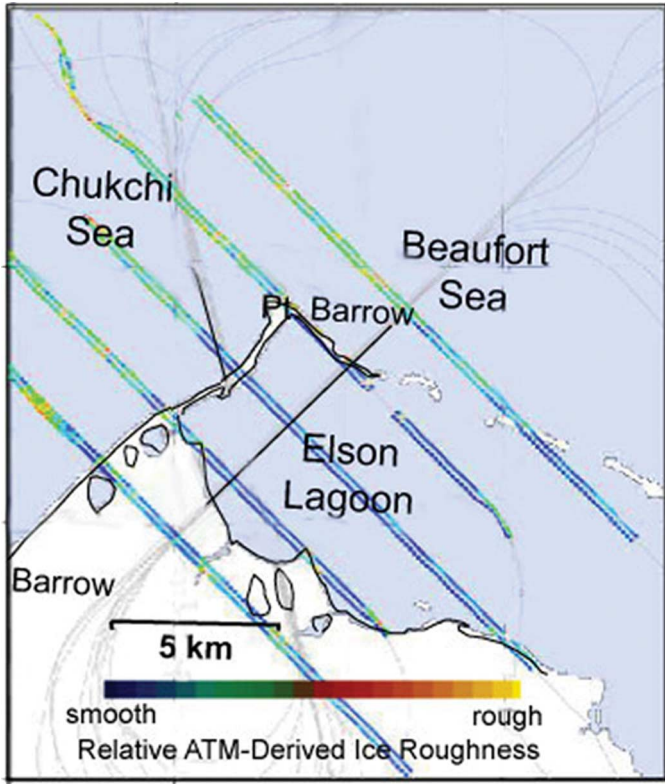


Fig. 4. ATM-derived surface roughness obtained during low-level passes of the NASA P-3. Relative degree of roughness is indicated by cool (smooth ice) versus warm (rough ice) colors. Transect locations (black lines) are shown as in the previous figures. Light-gray lines show the individual flight tracks of the NASA P-3 aircraft. Note the relatively smooth ice indicated in Elson Lagoon and the nearshore portion of the Chukchi Sea shore-fast ice, with roughest ice seen northeast of Point Barrow in the area of heavy ridging, within the *stamukhi* zone in the Chukchi area, and in the offshore pack ice.

TABLE I
ICE CONDITIONS WITHIN THE BARROW STUDY REGION AS CLASSIFIED BY MANUAL INTERPRETATION. ALSO INCLUDED ARE MEAN SAR BACKSCATTER, T_B , PR_i , $GR_{i,j}$, AND PSR-DERIVED SNOW DEPTH (H_s) FOR EACH CLASS. T_B ARE IN KELVIN. H_s IS IN CENTIMETERS

Class	SAR	$T_{B,21V,H}$	$GR_{27,10V}$	$GR_{37,10H}$	$GR_{19,10V}$	$GR_{19,10H}$	PR_{10}	PR_{19}	PR_{37}	H_s
ridged ice (red)	107	237, 217	-0.241	-0.124	0.010	0.004	0.050	0.054	0.045	22
Moderately rough ice within ice pack (dark red)	111	249, 227	-0.007	0.009	0.012	0.009	0.064	0.059	0.045	9
heavily rubbled ice (white)	97	240, 220	-0.019	-0.006	0.010	0.006	0.053	0.057	0.041	18
Moderately rubbled ice (black)	52	242, 217	-0.019	-0.009	0.010	0.010	0.064	0.063	0.053	18
lightly rubbled ice (yellow)	47	246, 223	-0.011	0.003	0.012	0.011	0.062	0.062	0.048	11
Moderately smooth ice (blue)	33	246, 223	-0.004	0.006	0.011	0.009	0.060	0.062	0.041	6
smooth ice (purple)	32	246, 223	-0.007	0.008	0.012	0.017	0.064	0.059	0.045	8

To better quantify these ice characteristics, we manually interpreted a fusion of SAR and gridded PSR imagery to delineate ice regimes corresponding to the patterns visible in the top panel in Fig. 3. The general ice conditions associated with each class are listed in Table I. These classes (shown in the bottom panel in Fig. 3) generally correspond to different roughness conditions as defined by the field observations, aerial photographs, and SAR imagery. Different roughness

TABLE II
CO-OCCURRENCE MATRIX OF THE MANUAL CLASSIFICATION SHOWN IN FIG. 3 VERSUS CLASSES DEFINED USING AN UNSUPERVISED K -MEANS CLUSTERING APPLIED TO PR_{10} , PR_{19} , AND PR_{37} . ASTERISK IN THE UNSUPERVISED CLASS LIST INDICATES THAT NO CLASS WAS IDENTIFIED CORRESPONDING TO THE MANUALLY DEFINED SMOOTH-ICE CLASS

Manually-defined classes:	Unsupervised classes:							
	1	2	3	4	5	*	7	N
1. ridged ice (red)	38	44	0	5	1		12	4469
2. heavily rubbled ice (white)	35	48	1	12			4	4172
3. moderately rubbled ice (black)	2	21	57	20	0		0	2449
4. lightly rubbled ice (yellow)	11	2	5	40	42			6998
5. moderately smooth ice (blue)	11	1	11	51	26		0	9380
6. smooth ice (purple)	14	0	0	40	46		0	661
7. moderately rough ice within ice pack (dark red)	7	27	1	3	1		60	4431

characteristics are associated with the ridging patterns in the Beaufort Sea, as shown by the pattern of classes 1 (red) and 2 (white) north and east of Point Barrow. Conditions within the ice pack in the Chukchi Sea, which are indicated by high SAR backscatter and relatively low T_B , appear unique compared with other areas and are assigned to a specific class (class 7; dark red). Higher backscatter for class 7 compared with rough ice within the shore-fast ice areas is due at least in part to the presence of wind-roughened or perhaps frost-flower-covered leads within the class 7 coverage. The areas of relatively rough ice with deeper snowpack within Elson Lagoon are assigned to a separate class (class 3; black). To help avoid biasing the manual interpretation to conform to any predetermined view of ice conditions, a portion of the available information, such as the ATM roughness data and the PSR-derived snow depths described later, were not referred to when constructing the manual mapping of classes. These data thus provide an independent check of the classification. In addition, unsupervised classification of the same image channels using an ENVI software implementation of K -means clustering [20] yields similar class delineations, indicating that the manual classification faithfully represents the conditions exhibited in the SAR + PSR composite (Table II).

Although spatial patterns in T_B are clearly associated with ice conditions, the range of T_B for different ice categories is relatively small, particularly in comparison to the range in SAR backscatter. For example, $T_{B,10V}$ vary by about 8 K between the lowest and highest T_B over sea ice. At $T_{B,37V}$, the maximum range of T_B for different ice conditions (limited to areas of 100% ice) increases to about 15 K. Differences are greatest in the horizontally polarized channels, consistent with previous findings (e.g., [21] and [22]). Mean T_B and ratios summarized for each of the ice classes in Fig. 3 are provided in Table I along with normalized polarization ratio (PR) and gradient ratio (GR) defined as follows:

$$PR_i = (T_{B,i,V} - T_{B,i,H}) / (T_{B,i,V} + T_{B,i,H}) \quad (1)$$

$$GR_{i1,i2,j} = (T_{B,i1j} - T_{B,i2j}) / (T_{B,i1j} + T_{B,i2j}) \quad (2)$$

where $i1$ and $i2$ are frequencies at polarization j .

B. Relationships Between Snow Depth and Ice Conditions

One of the validation tasks for which the *in situ* component of AMSR-Ice03 was specifically designed is evaluation of the

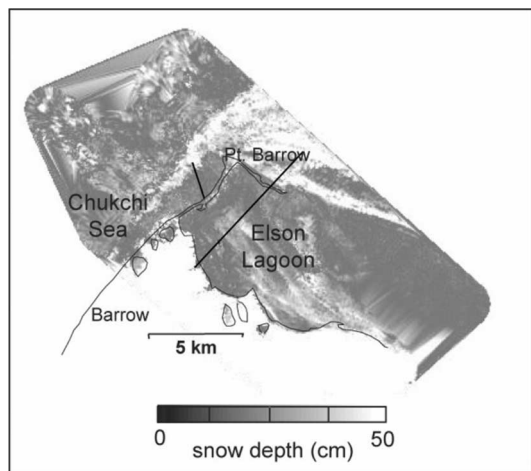


Fig. 5. PSR-derived snow depth for the Barrow study area. The patterns in the upper left of the image are artifacts of the PSR sampling and gridding process. Coastline and transect locations (heavy black lines) are shown, as in previous figures.

AMSR-E snow-on-sea-ice algorithm. Markus *et al.* [23] describe this snow algorithm in detail as well as its application to the AMSR-Ice03 data, but in brief, the basis of the algorithm is that snow preferentially scatters microwave emission at higher frequencies compared with lower frequencies. The algorithm is based on $GR_{37,19V}$ and, at present, is applicable only to first-year ice areas and not to multiyear ice since a method has not yet been devised to differentiate between GR variations due to snow versus those due to the multiyear ice itself. $GR_{37,19V}$ becomes increasingly negative as snow depth increases. In the top panel in Fig. 3, this gradient effect is most obvious over areas such as Elson Lagoon, where the brighter green tones correspond to deeper snow. Snow depth (H_s) calculated using PSR data converted to AMSR-equivalent T_B using regression coefficients provided by Markus *et al.* [23] is shown for the full study area (Fig. 5). Fig. 5 depicts a considerable range in estimated snow depth, with deepest snow indicated over the ridged and rubble ice extending from the *stamukhi* zone in the Chukchi Sea to the northeast and east around Point Barrow. Snow depth is variable in Elson Lagoon, which, as noted earlier, presented a fairly uniform appearance during initial field reconnaissance and in aerial photographs. Using the results of the manual classification, PSR-derived snow depth statistics were calculated for each of the mapped classes (Table I). Mean T_B , GR, and PR values for each class are also included in Table I. Since the snow depth algorithm relies on an expected relationship between volume scattering and snow depth, other snowpack conditions that affect scattering such as presence of depth hoar or ice lenses will influence the algorithm results. Details of snowpack conditions and effects are provided by Sturm *et al.* [2] and Markus *et al.* [23].

Sturm *et al.* [2] find a strong correlation between surface roughness and snow accumulation along the field transects. Comparison of the measured snow depth data with PSR-derived snow depth along the transects (Figs. 6–8) demonstrates good agreement between the measured and PSR-estimated snow depth for the Chukchi and Elson transects, but with greater differences for the Beaufort transect. Mean observed snow depths

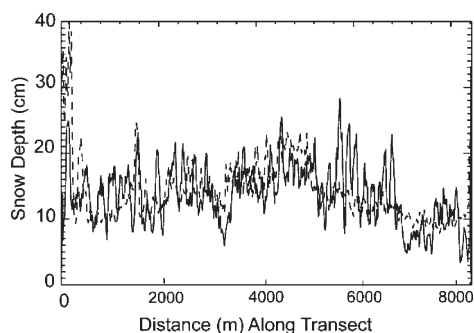


Fig. 6. Comparison of measured (solid line) and PSR-derived (dashed line) snow depths for the Elson transect. The measured snow depths are smoothed with a 20-sample running mean.

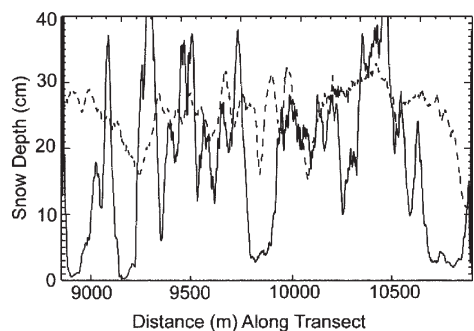


Fig. 7. Comparison of measured (solid line) and PSR-derived (dashed line) snow depths for the Beaufort transect. The measured snow depths are smoothed with a 20-sample running mean.

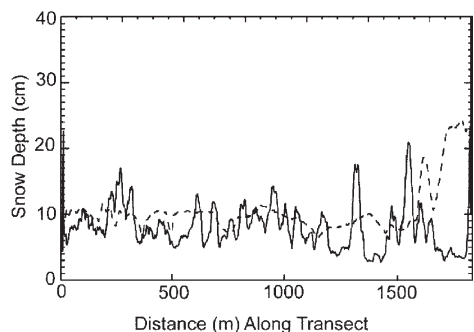


Fig. 8. Comparison of measured (solid line) and PSR-derived (dashed line) snow depths for the Chukchi transect. The measured snow depths are smoothed with a 20-sample running mean.

averaged over the Chukchi, Beaufort, and Elson transects are 8.1, 19.1, and 14.0 cm, respectively, with a small portion of the transects on and adjacent to land excluded. The corresponding PSR-derived mean snow depths are 10.3, 25.7, and 13.8 cm, respectively. If the northwestward-most portion of the Chukchi transect where ice roughness is considerably greater than over the rest of the transect is excluded, the mean snow depths for the remainder of the Chukchi transect are 8.4 and 9.5 cm for the observed and PSR-derived values, respectively. Markus *et al.* [23] provide further results comparing the measured and PSR-derived snow depths, as well as the relationships to ice roughness.

The PSR-derived snow depths reproduce the overall variability as well as the magnitude of snow depth along the transect. Based on this agreement, Figs. 3 and 5–8 can be used to illustrate how the snow depths relate to the broader spatial

patterns. The area of deeper snow encountered along the *in situ* transect in the center of Elson Lagoon (Fig. 6) is seen to be part of a general pattern of deeper snow within the lagoon, as is apparent in Fig. 5. Comparison to the SAR data shows that this is also a location of higher backscatter and is classified as “lightly rubbled” ice in Fig. 3. As described by Sturm *et al.* [2], snow drifts were considerably larger in this portion of Elson Lagoon. Herzfeld *et al.* [19] show that the lagoon’s snowpack can be divided into several distinct zones based on roughness. ATM-derived height variations were small for this portion of the track, indicating that the variation in snow depth did not translate into a clear variation in surface height profile, within the detection limits of the laser.

The poorer agreement between observed and PSR-derived snow depths in the Beaufort Sea transect (Fig. 7) can be attributed to effects of the rougher ice in this area. The deeper snow and rougher surface compared with the Elson and Chukchi transects are part of the ridge/rubble complex north of the Point Barrow spit and extend to the east and northeast. Ice in this portion of the transect was very rough, with a complex ridge of about 4 m height at the southern end of the segment, numerous blocks of upthrust and overthrust ice further north along the transect, and with occasional small pans of smooth ice. While this large-scale roughness results in reduced correlation between observed and PSR-derived snow depth along the transect (Fig. 7), some of this lack of correlation is due to the effects of the relatively large pixel sizes in the PSR data. In fact, the difference of 6.6 cm in mean snow depths (PSR minus observed) averaged over the transect is not as great as might have been expected given the lack of spatial correlation.

The snow depth profile and PSR-derived snow depths on the Chukchi Sea transect (Fig. 8) show a slight overestimate in the PSR data. In this location, the lack of variability observed in the ATM data and the low SAR backscatter support the conclusion by Sturm *et al.* [2] that the surface in this location was the smoothest encountered in the study domain (with the exception of a few isolated pans of refrozen ice or possibly small floes trapped within the Beaufort area). As with the transition point between the Elson and Beaufort ice, roughness and snow depth increase at the northwestward end of the Chukchi transect, within rubble and adjacent to a ridge. The PSR data indicate that snow depth is uniform and shallow over the entire interior portion of the Chukchi Sea shore-fast ice shoreward of the *stamukhi* zone. This is consistent with the fact that ice in this location had sheared free of land in January, with subsequent formation of ice simultaneously over this entire area.

Summarizing PSR-derived snow depths for each of the manually delineated ice classes (Table I) helps to quantify the observed relationship between ice roughness/complexity and snow depth. Snow depth decreases as the ice becomes smoother, from a mean of 22 cm within the ridged-ice area to a mean of 6–8 cm for the moderately smooth and smooth-ice categories.

C. Relationships of Brightness Temperatures to Ice Roughness and Other Factors

As has been demonstrated in previous studies, e.g., Wensnahan *et al.* [24], Eppler *et al.* [3], and Hallikainen and Winebrenner [6], PR varies depending on ice conditions. Most of this previous work has focused on effects during the

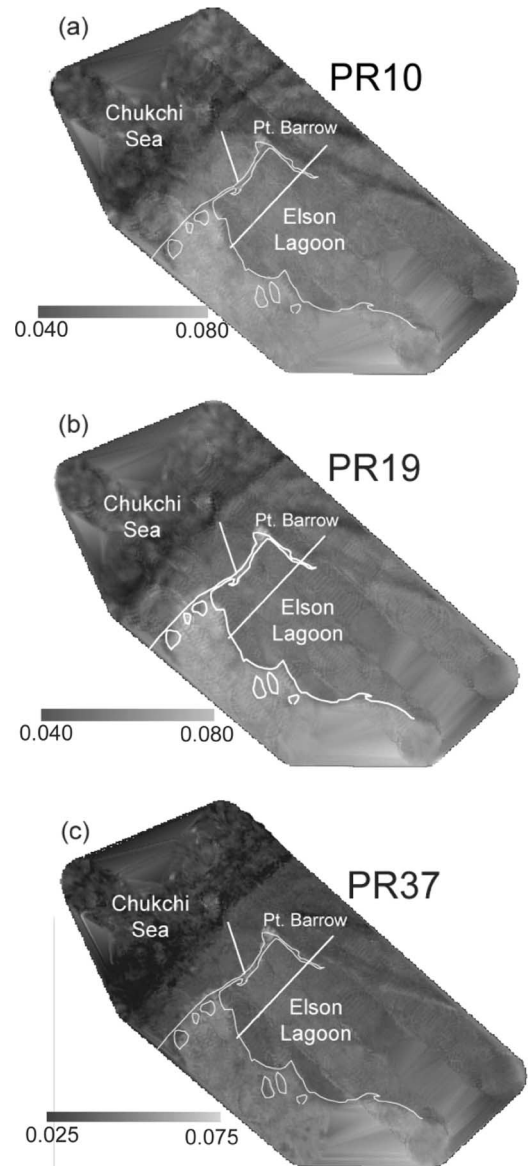


Fig. 9. Comparison of (a) PR₁₀, (b) PR₁₉, and (c) PR₃₇. Lowest PR regions vary with frequency and appear to correspond to different ice roughness conditions.

transition from open water to new and young ice. Here, and in Markus *et al.* [23], the relationships to ice roughness are considered. Comparison of PR at 10, 19, and 37 GHz for the Barrow area (Fig. 9) shows spatial relationships that appear associated with ice conditions, with each frequency responding differently within different areas of the ice cover. The lowest PR₁₀ values (excluding the pack ice where some open water and thin ice are present) correspond to the “heavily rubbled ice” and “ridged-ice” classes in Fig. 3. PR₁₉ is similar but with some of the ridged/rubbled areas (such as those aligned with the barrier islands to the east of Point Barrow) less distinct at 19 GHz. Variations in PR₃₇ are primarily between pack ice and shore-fast ice. Individual floes within the pack ice can be seen due to their consistent PR values across frequency. One interpretation of these patterns is that depolarization (an increase in H-polarized relative to V-polarized emission) is sensitive to the nature of ice roughness, with this sensitivity dependent on frequency. Given the greater penetration depth

at 10 GHz, PR_{10} may be affected most by heavily ridged ice with its complex matrix of blocks of ice and gaps. At 37 GHz, emission is from nearer the snow/ice surface, such that PR_{37} is relatively insensitive to variations deeper within the ice structure. The addition of a snow pack would also tend to mask underlying ice roughness at 37 GHz [6], but with less of an effect at the lower frequencies. This masking is less significant over the pack-ice portion of the study area where snow depth is less (as indicated by the PSR-derived snow depths in Fig. 5 and based on likely ice age).

Farmer *et al.* [8] present a conceptual model of ridge formation and aging that highlights the importance of snow accumulation in modifying the microwave signature of ridges. In addition to the direct effects of snow trapping and accumulation within ridges that then affect microwave emissivity, they point out that other processes such as metamorphism of snow and of exposed ice in ridged-ice blocks and formation of hoar crystals within open cavities in ridges and rubble would further act to reduce emissivity. Such scattering along with scattering from a complex layered snow pack within rough-ice zones could be expected to be most obvious in horizontally polarized T_B . This would help explain the polarization differences shown in Fig. 9. One would expect that this combination of factors would also yield an increase in spectral gradient (e.g., $GR_{37,19V}$), yielding overestimates in snow depth. These factors also likely contribute to the decrease in correlation between snow depth and $GR_{37,19V}$ within rough ice described by Markus *et al.* [23].

These effects also raise the question as to whether ridged and rubble ice, independent of snow accumulation, might increase spectral gradient and in turn produce overestimates in microwave-derived snow depth in areas of rough ice. The fact that the AMSR-E snow depth algorithm as applied to the PSR data results in shallow snow depths over the rough pack ice indicates that the GR is relatively unaffected by this degree of roughness (excluding the role of roughness in trapping snow). This would be fortunate since, otherwise, rough ice (independent of snow cover) would contribute to errors in estimated snow depth. On the other hand, if increased roughness decreases PR, as discussed in the next section, this would introduce an overestimate in total ice concentration in the existing passive microwave algorithms (or an underestimate for smooth ice, depending on the algorithm coefficients or tie points used). More detailed study of microwave signatures of rough ice with and without deep snow packs is needed along with radiometric modeling of rough ice and snow to help resolve this uncertainty. Unfortunately, accurate simulations of the complex and chaotic mixtures and layering of different forms of ice, air pockets, and snow within rough ice zones remain problematic. It is worth pointing out that the ice present in the Chukchi *stamukhi* zone and offshore of Point Barrow may be rougher and more complex than is typical of ridging and rubbing in most pack-ice areas. However, there are relatively few comprehensive sets of roughness observations over a full range of pack-ice conditions to confirm this.

Application of unsupervised K -means clustering [20] to a three-channel image formed from the PR data (PR_{10} , PR_{19} , and PR_{37}) yields classes (Fig. 10) that correspond well to the roughness categories defined by the manual classification presented earlier in terms of spatial distribution (Fig. 3) and

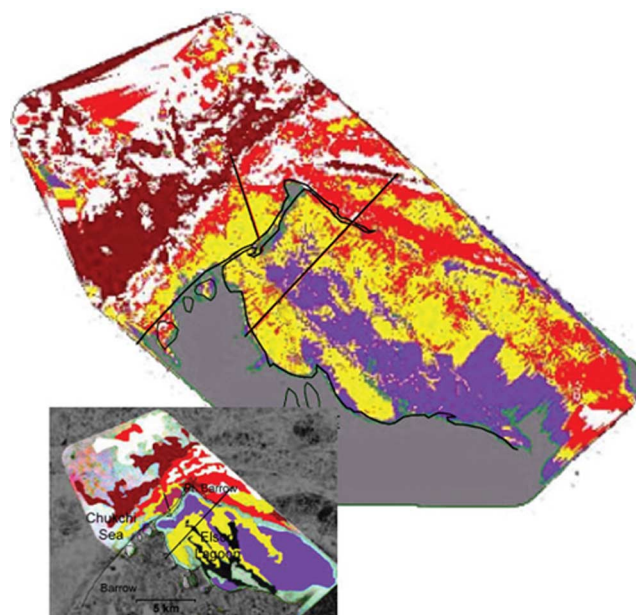


Fig. 10. Results of an unsupervised clustering of PR_{10} , PR_{19} , and PR_{37} . The color assignments correspond to those in Fig. 3 and Table III. The manually classified map shown in Fig. 3 is included here as an inset for comparison.

TABLE III
MEAN PRS ASSOCIATED WITH EACH OF THE CLASSES SHOWN IN FIG. 10

Class	PR_{10}	PR_{19}	PR_{37}
1. <u>ridged ice</u> (red)	0.055	0.060	0.046
2. <u>heavily rubbled ice</u> (white)White (2)	0.050	0.054	0.040
4. <u>lightly rubbled ice</u> (yellow)	0.061	0.062	0.048
5. <u>moderately smooth ice</u> (blue)	0.065	0.066	0.054
7. <u>moderately rough ice within ice pack</u> (dark red)	0.044	0.048	0.030

class assignment (Table I). For example, the classes located over ridged and heavily rubbled ice are nearly equally divided between the ridged and rubbled ice classes [classes 1 (red) and 2 (white)] in the manual classification. The only notable discrepancy is that the unsupervised classification does not identify a specific class corresponding to the smooth-ice category in the manual classification, which can be explained by the fact that the SAR data were not included as a data channel in the unsupervised classification. This general agreement between manually defined classes and the PR-based classes support the contention that PR is well correlated with ice roughness, at least on the scales considered here.

Mean polarization values for each of the classes in Fig. 10 are provided in Table III and are similar to those summarized for the manually derived classes (Table I). Note also that within the pack ice, the PR images show features that correspond to ice floes based both on shape and on comparison with the SAR data. For such floes, the relatively high polarization in each channel along with low backscatter suggest that these are smooth-ice features.

As mentioned above, effects of roughness on PR could be expected to translate into errors in ice concentration

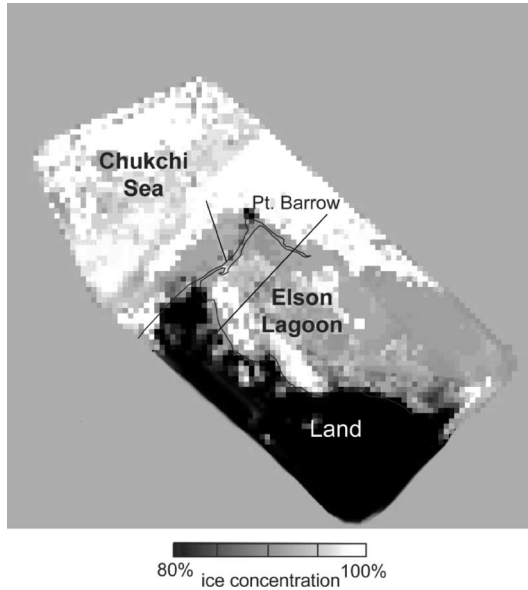


Fig. 11. Total ice concentration calculated using the NT-2 algorithm applied to PSR data (data shown here were subsampled by four to reduce computation time).

estimated using algorithms that employ PR ratios. The NT-2 sea-ice algorithm, when applied to the PSR data (regressed to approximate AMSR-E T_B using the coefficients provided by Markus *et al.* [23]), shows this apparent sensitivity to the effects of rougher ice on PR (Fig. 11). The relatively smooth ice in Elson Lagoon and the Chukchi nearshore fast ice have PSR-derived concentrations averaging about 90%, versus 100% in the roughest ice locations. The lowest estimated concentration within the shore-fast ice was 83%. Actual concentrations were 100% within all the fast ice areas, with some new leads present in the pack ice offshore of the Chukchi *stamukhi* zone. The NT-2 algorithm defaults to 100% when the algorithm generates concentrations greater than 100%; thus, further analysis is needed to see what the effects might be when mixtures of open water and rough ice are present. Mean concentration for each of the classes in Fig. 3 and Table I are 98% (class 1), 98% (class 2), 91% (class 3), 93% (class 4), 91% (class 5), 92% (class 6), and 98% (class 7). Ice that is smooth to moderately rubbled exhibits little effect of roughness on derived concentration: the positive biases are confined to the roughest ice classes. Again, as noted above, the ice observed in the study area may be considerably rougher than is typical for pack ice; thus, the concentration errors seen here may be larger than would be usual over most of the sea-ice cover. Estimates of multiyear ice using $GR_{37,19V}$ will also be affected, either directly or through the effects of enhanced snow trapping by rough ice. The most likely effect would be to cause an overestimate in multiyear ice fraction when rough ice is present, but this remains to be determined. More detailed observations of surface roughness, ice morphology, and snow depth over a range of pack-ice conditions are needed to test these assumptions regarding total and multiyear ice concentration.

In addition to the conclusions regarding variations in ice and snow emissivity, it is worth noting that the PSR data show strong T_B contrasts between land and sea ice, even in a location such as Barrow where the ground is frozen and similar snow pack is present on ice and adjacent land. “Ice concentration”

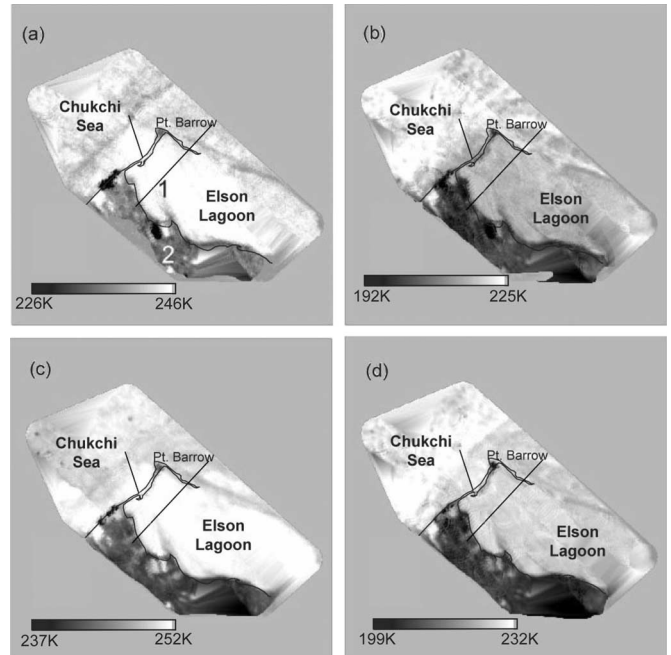


Fig. 12. (a) $T_{B,10V}$, (b) $T_{B,10H}$, (c) $T_{B,19V}$, and (d) $T_{B,19H}$. Locations of relict lake shoreline (1) and lakes with different emissivities (East and West Twin Lakes) (2) are labeled in (a).

estimated by the NT-2 algorithm over land (such as would occur in mixed pixels or due to geolocation error) is 79% on average, indicating the typical magnitude of error that could be expected to be introduced by land contamination in AMSR-E coastal pixels.

In addition to the larger issues of retrievals of snow depth and effects of roughness, the PSR data acquired in the Barrow area during AMSR-Ice03 show a number of features that are of less interest for satellite applications but are intriguing nonetheless. For example, the data show differences in lake ice conditions. $T_{B,10.7V}$ and $T_{B,19V}$ in Fig. 12 depict T_B differences between two adjacent lakes (“West and East Twin Lakes”), most likely indicating that one of the lakes was frozen to the lake bed. Weeks *et al.* [25] and Jeffries *et al.* [26] describe this phenomenon as seen in radar imagery. Another interesting result is the apparent correspondence between $T_{B,10.7V}$ and $T_{B,19V}$ PSR data and areas where the ice is likely to be grounded (locations where the ice has frozen solid to the seabed). This is shown in Fig. 12 as reduced T_B over a relict lake shoreline extending into Elson Lagoon, forming the northeastern portion of the drained lake that is apparent in the shape of the lagoon. This is a location where ice is known by Barrow residents to freeze down to the seabed. A similar pattern occurs in the Chukchi Sea and at the northern edge of Elson Lagoon in likely grounding locations. Even at 10 GHz though, the penetration depth of saline ice is small; thus, other factors are presumably at work to produce the observed T_B patterns. It was noted earlier that these locations are areas of ridging, and other possible effects of grounding on ice roughness are discussed by Gray *et al.* [18].

IV. CONCLUSION

Detailed *in situ* observations and field reconnaissance, aircraft-acquired PSR microwave imagery, RADARSAT SAR

backscatter data, airborne laser profilometry, and a variety of other supporting information were combined to study how Barrow-area sea-ice conditions affect passive microwave brightness temperatures, measures such as microwave spectral ratio and PR and microwave-derived estimates of snow depth and ice concentration. Good agreement is found between measured snow depths and snow depths estimated using the AMSR-E algorithm applied to the PSR microwave data over smooth to moderately rough ice. The ability to extrapolate *in situ* point measurements to a broader area and to specific ice regimes supports the findings of other papers in this special issue regarding the strong correlation between ice roughness and snow depth. The mapping illustrates details about the formation processes and history of the shore-fast ice zone, including contrasts with adjacent pack ice. Snow depths are found to range from a mean of 22 cm over the most complex, ridged ice to 6 cm over relatively young undeformed ice. Relationships are also seen between ice conditions and corresponding variations in polarization. Comparison of PRs at 10, 19, and 37 GHz suggests that each channel responds differently to degrees of ridging and roughness. This effect on PR translates into possible overestimates of ice concentration by about 10% for the ice conditions in the study area (100% first-year ice with moderate and variable snow pack). This may not be typical of errors elsewhere in the Arctic since the range of ice roughness encountered in the study area may be more extreme than is usual for pack ice and most shore-fast ice areas.

ACKNOWLEDGMENT

The authors would like to thank the contribution of the entire team participating in AMSR-Ice03 effort, including field and aircraft crews; the Barrow Arctic Science Consortium for logistics support; and the invaluable contributions of members of the Barrow community to this study and to polar research over many years. RADARSAT data were provided by the Alaska SAR Facility, courtesy of RADARSAT International, Inc.

REFERENCES

- [1] T. C. Grenfell, "Surface-based passive microwave studies of multiyear sea ice," *J. Geophys. Res.*, vol. 97, no. C3, pp. 3485–3501, 1992.
- [2] M. Sturm, J. A. Maslanik, D. K. Perovich, J. C. Stroeve, J. Richter-Menge, T. Markus, J. Holmgren, J. F. Heinrichs, and K. Tape, "Snow depth and ice thickness measurements from the Beaufort and Chukchi Seas collected during the AMSR-Ice03 campaign," *IEEE Trans. Geosci. Remote Sens.*, vol. 44, no. 11, pp. 3009–3020, Nov. 2006.
- [3] D. T. Eppler, "Passive microwave signatures of sea ice," in *Geophys. Remote Sens. Sea Ice*, ser. Geophysical Monograph, F. D. Carsey, Ed. Washington, DC: Amer. Geophys. Union, 1992, vol. 68, ch. 4, pp. 47–71.
- [4] T. C. Grenfell, M. R. Wensnahan, and D. P. Winebrenner, "Passive microwave signatures of simulated pancake ice and young pressure ridges," *Remote Sens. Rev.*, vol. 9, pp. 51–64, 1994.
- [5] R. Kwok, S. V. Nghiem, S. Martin, D. P. Winebrenner, A. J. Gow, D. K. Perovich, C. T. Swift, D. G. Barber, K. M. Golden, and E. Knapp, "Laboratory measurements of sea ice: Connections to microwave remote sensing," *IEEE Trans. Geosci. Remote Sens.*, vol. 36, no. 5, pp. 1716–1730, Sep. 1998.
- [6] M. Hallikainen and D. P. Winebrenner, "The physical basis for sea ice remote sensing," in *Geophys. Remote Sens. Sea Ice*, ser. Geophysical Monograph, F. D. Carsey, Ed. Washington, DC: Amer. Geophys. Union, 1992, vol. 68, ch. 3, pp. 29–46.
- [7] D. P. Winebrenner *et al.*, "Passive microwave signatures of sea ice," in *Geophysical Remote Sensing of Sea Ice*, ser. Geophysical Monograph, F. D. Carsey, Ed. Washington, DC: Amer. Geophys. Union, 1992, vol. 68, ch. 4, pp. 137–175.
- [8] D. L. Farmer, D. T. Eppler, and A. W. Lohanick, "Passive microwave signatures of fractures and ridges in sea ice and 33.6 GHz (vertical polarization) as observed in aircraft images," *J. Geophys. Res.*, vol. 98, no. C3, pp. 4645–4665, 1995.
- [9] A. W. Lohanick, "Some observations of established snow cover on saline ice and their relevance to microwave remote sensing," in *Sea Ice Properties and Processes*, S. F. Ackley and W. W. Weeks, Eds. Hanover, NH: Cold Regions Res. Eng. Lab., 1991, pp. 61–67. CRREL Monograph 90-1.
- [10] D. J. Cavalieri, T. Markus, J. A. Maslanik, M. Sturm, and E. Lobl, "March 2003 EOS Aqua AMSR-E arctic sea ice field campaign," *IEEE Trans. Geosci. Remote Sens.*, vol. 44, no. 11, pp. 3003–3008, Nov. 2006.
- [11] J. R. Piepmeier and A. J. Gasiewski, "Polarimetric Scanning Radiometer for airborne microwave imaging studies," in *Proc. IGARSS*, Lincoln, NE, May 27–31, 1996, pp. 1688–1691.
- [12] A. K. Jordan and M. E. Veysoglu, "Electromagnetic remote sensing of sea ice," *Inv. Probl.*, vol. 10, no. 5, pp. 1041–1058, 1994.
- [13] W. R. Krabill, R. H. Thomas, C. F. Martin, R. N. Swift, and E. B. Frederick, "Accuracy of airborne laser altimetry over the Greenland ice sheet," *Int. J. Remote Sens.*, vol. 16, no. 7, pp. 1211–1222, 1995.
- [14] W. Krabill, E. Frederick, S. Manizade, C. Martin, J. Sonntag, R. Swift, R. Thomas, W. Wright, and J. Yungel, "Rapid thinning of parts of the southern Greenland ice sheet," *Science*, vol. 283, no. 5407, pp. 1522–1524, 1999.
- [15] M. Belmonte Rivas, J. A. Maslanik, J. G. Sonntag, and P. Axelrad, "Sea-ice roughness from airborne LIDAR profiles," *IEEE Trans. Geosci. Remote Sens.*, vol. 44, no. 11, pp. 3032–3037, Nov. 2006.
- [16] J. A. Maslanik, J. Curry, S. Drobot, and G. Holland, "Observations of sea ice using a low-cost unpiloted aerial vehicle," in *Proc. 16th. Int. Symp. Sea Ice IAH*, 2002, vol. 3, pp. 283–287.
- [17] J. A. Curry, J. A. Maslanik, G. Holland, J. Pinto, G. Tyrrell, and J. Inoue, "Applications of aerosondes in the Arctic," *Bull. Amer. Meteorol. Soc.*, vol. 85, no. 12, pp. 1855–1861, 2004.
- [18] A. L. Gray, R. K. Hawkins, C. E. Livingstone, L. Drapier Aresenault, and W. M. Johnstone, "Simultaneous scatterometer and radiometer measurements of sea-ice microwave signatures," *IEEE J. Ocean. Eng.*, vol. 7, no. 1, pp. 20–32, Jan. 1982.
- [19] U. C. Herzfeld, J. A. Maslanik, and M. Sturm, "Geostatistical characterization of snow-depth structures on sea ice near point Barrow, Alaska—A contribution to the AMSR-Ice03 field validation campaign," *IEEE Trans. Geosci. Remote Sens.*, vol. 44, no. 11, pp. 3038–3056, Nov. 2006.
- [20] J. T. Tou and R. C. Gonzalez, *Pattern Recognition Principles*. Reading, MA: Addison-Wesley.
- [21] H. J. Zwally, J. C. Comiso, C. L. Parkinson, W. J. Campbell, F. D. Carsey, and P. Gloersen, "Antarctic sea ice, 1973–1976: Satellite passive-microwave observations," NASA, Washington, DC, NASA SP-459, 1983.
- [22] P. Gloersen, W. J. Campbell, D. J. Cavalieri, J. C. Comiso, C. L. Parkinson, and H. J. Zwally, "Arctic and Antarctic sea ice, 1978–1987: Satellite passive-microwave observations and analysis," NASA, Washington, DC, NASA SP-511, 1992.
- [23] T. Markus, D. J. Cavalieri, A. J. Gasiewski, M. Klein, J. A. Maslanik, D. C. Powell, B. Stankov, J. C. Stroeve, and M. Sturm, "Microwave signatures of snow on sea ice: Observations," *IEEE Trans. Geosci. Remote Sens.*, vol. 44, no. 11, pp. 3081–3090, Nov. 2006.
- [24] M. Wensnahan, T. C. Grenfell, D. P. Winebrenner, and G. A. Maykut, "Observations and theoretical studies of microwave emission from thin saline ice," *J. Geophys. Res.*, vol. 98, no. C5, pp. 8531–8546, 1993.
- [25] W. F. Weeks, A. G. Fountain, M. L. Bryan, and C. Elachi, "Differences in radar returns from ice-covered North Slope lakes," *J. Geophys. Res.*, vol. 83, no. C8, pp. 4069–4073, 1978.
- [26] M. O. Jeffries, K. Morris, W. F. Weeks, and H. Wakabayashi, "Structural and stratigraphic features and ERS-1 synthetic aperture radar backscatter characteristics of ice growth on shallow lakes in NW Alaska winter 1991–1992," *J. Geophys. Res.*, vol. 99, no. C11, pp. 22 459–22 474, 1994.



James A. Maslanik received the B.S. degree in forest science and the M.S. degree in environmental pollution control from the Pennsylvania State University, University Park, PA, in 1980 and 1978, respectively, and the Ph.D. degree in geography from the University of Colorado, Boulder, in 1984.

He is a Research Professor with the Department of Aerospace Engineering Sciences, University of Colorado. His research interests include the interactions of sea ice with atmosphere and ocean, remote sensing and field investigations of sea-ice properties, effects of climate change on Arctic coastal communities, and development and deployment of unpiloted aerial vehicles for polar research.



Matthew Sturm received the M.S. and Ph.D. degrees in geophysics from the University of Alaska, Fairbanks, AK, in 1984 and 1989, respectively.

He is currently a Research Scientist with the U.S. Army Cold Regions Research and Engineering Laboratory-Alaska, Fort Wainwright, AK. He has led over 15 Arctic expeditions. His research interests include Arctic climate change, snow on land, and snow on sea ice.

Dr. Sturm is a member of the American Geophysical Union, the International Glaciological Society, and the Arctic Institute of North America.



John F. Heinrichs (M'06) received the B.S. and M.S. degrees in mathematics from the University of Wisconsin-Milwaukee (UWM), Milwaukee, in 1983 and 1985, respectively, and the Ph.D. degree in geography from the University of Colorado, Boulder, in 1996.

He was a Staff Scientist with the Hughes Aircraft Company from 1986 to 1992, a Research Assistant with the Cooperative Institute for Research in Environmental Sciences (CIRES), Boulder, from 1992 to 1996, and a Postdoctoral Researcher with CIRES from 1996 to 1998. Since 1998, he has been with the faculty of Fort Hays State University, Hays, KS, where he is currently an Associate Professor and the Chair of the Department of Geosciences.

Dr. Heinrichs is a member of the IEEE Geoscience and Remote Sensing Society, the American Geophysical Union, and the Association of American Geographers.



Maria Belmonte Rivas received the B.S. and M.S. degrees in Earth physics from the Universidad Complutense de Madrid, Madrid, Spain, in 1999. She is currently working toward the Ph.D. degree in aerospace engineering at the University of Colorado, Boulder.

From 2000 to 2003, she worked at the European Space Agency, The Netherlands, on the utilization of reflected signals from global navigation satellite systems (GNSS) for sea-level monitoring. Her current research focuses on the analysis of scattered GNSS

signals from Arctic sea ice.

Ms. Rivas was awarded the National Aeronautics and Space Administration Earth System Science Fellowship toward the completion of her doctoral studies, in 2004.



Ute C. Herzfeld received a master-level degree in mathematics, evangelical theology, and education (Staatsexamen) from the Johannes Gutenberg Universitaet Mainz, Mainz, Germany, in 1983, the Ph.D. degree in mathematics with applied mathematics and geosciences from the Universitaet Mainz, Mainz, in 1986, and a Postgraduate Diploma in geomathematics from the Free University of Berlin, Berlin, Germany, in 1986. She also studied mathematics and philosophy at the University of Warwick, Coventry, U.K., and took a postgraduate course in oceanography at the Universitaet Kiel, Germany.

She is currently a Senior Research Associate with the Cooperative Institute for Research in Environmental Sciences, University of Colorado, Boulder, CO. Since 1995, she has been Head of the Geomathematics Division of the Universitaet Trier, Germany. She is a Geomathematician and Glaciologist with 20 years of experience in the analysis of remote-sensing data and extensive field experience in high-latitude glaciers and ice streams, including expeditions to Antarctica, Greenland, and Alaska. She is an Associate Editor of *Computers & Geosciences* and has published three books and 88 scientific papers in international journals.

Prof. Herzfeld was awarded the President's Prize of the International Association for Mathematical Geology for outstanding contributions in theoretical and applied geostatistics.



Albin J. Gasiewski (S'81-M'88-SM'95-F'02) received the B.S. and M.S. degrees in electrical engineering and the B.S. degree in mathematics from Case Western Reserve University, Cleveland, OH, in 1983, and the Ph.D. degree in electrical engineering and computer science from the Massachusetts Institute of Technology, Cambridge, in 1989.

He is a Professor of electrical and computer engineering with the University of Colorado at Boulder and the Director of the CU Center for Environmental Technology. From 1989 to 1997, he was a Faculty

Member with the School of Electrical and Computer Engineering at the Georgia Institute of Technology, where he became an Associate Professor. From 1997 to 2005, he was with the U.S. National Oceanic and Atmospheric Administration's (NOAA) Environmental Technology Laboratory in Boulder, CO, where he was the Chief of the ETL's Microwave Systems Development Division. He has developed and taught courses on electromagnetics, remote sensing, instrumentation, and wave propagation theory. His technical interests include passive and active remote sensing, radiative transfer, antennas and microwave circuits, electronic instrumentation, meteorology, and oceanography.

Prof. Gasiewski is the Past President (2004-2005) of the IEEE Geoscience and Remote Sensing Society. He is a member of the American Meteorological Society, the American Geophysical Union, the International Union of Radio Scientists (URSI), Tau Beta Pi, and Sigma Xi. He currently serves as Vice Chair of USNC/URSI Commission F. He served on the U.S. National Research Council's Committee on Radio Frequencies (CORF) from 1989-1995. He is the General Cochair of IGARSS 2006, to be held in Denver, CO.



Jon Holmgren received the B.S. degree in geology/geophysics from the University of Alaska-Fairbanks, Fairbanks, in 1987.

He is a Research Scientist with the U.S. Army Cold Regions Research and Engineering Laboratory-Alaska, Ft. Wainwright, where he develops instrumentation and apparatus for field and experimental projects, and operates a commercial machine shop. He has extensive experience in making measurements on sea ice.



Marian Klein (M'95) received the M.S. and Ph.D. degrees in electrical engineering from Technical University of Košice (TU Košice), Košice, Slovak Republic, in 1986 and 1996, respectively.

From 1987 to 1996, he was a member of the Faculty of Electrical Engineering and Informatics, TU Košice. From September 1996 to June 1997, he was a Fulbright Scholar with Georgia Institute of Technology, where he worked on the Laboratory for Radio Science and Remote Sensing. Since August 1998, he has been a Research Associate with the Cooperative Institute for Research in Environmental Sciences, University of Colorado, Boulder. He is also the Laboratory Manager for the CU Center for Environmental Technology. He has extensive knowledge and experience in radiometer systems design for harsh environments, whether airborne or ground based. He successfully led many field deployments of radiometric systems, which were used in many experiments of the National Aeronautics and Space Administration, the National Oceanic and Atmospheric Administration (NOAA), the Department of Energy, and the Department of Defense including several Soil Moisture Experiments (1999, 2002, 2003, and 2004), the Wakasa Bay experiment (2003), the Cold Land Processes Experiments (2002 and 2003), and AMSR-E Arctic and Antarctic Sea Ice Experiments (2003 and 2004). He was a Project Leader for the Ground-based Scanning Radiometer deployed in Barrow, Alaska, in 2004. He is a Lead Field Engineer and Design and Fabrication Leader for several instruments of the NOAA/Environmental Technology Laboratory and the Center for Environmental Technology, such as the Polarimetric Scanning Radiometer system including its PSR-A, PSR-CX, and PSR-S scanheads. He is also currently the Chief Executive Officer of Boulder Environmental Sciences and Technology, LLC. His research interests include passive microwave remote sensing, radiative transfer theory, and development of millimeter- and submillimeter-wave instrument systems for environmental studies.



Thorsten Markus (M'05) received the M.S. and Ph.D. degrees in physics from the University of Bremen, Bremen, Germany, in 1992 and 1995, respectively.

He is currently a Research Scientist with the NASA Goddard Space Flight Center (GSFC), Greenbelt, MD. From 1995 to 1996, he was a National Research Council Resident Research Associate with GSFC before joining NASA-UMBC Joint Center for Earth Systems Technology, where he worked until 2002. His research interests include satellite microwave remote sensing of primarily ice and the utilization of satellite data to study oceanic and atmospheric processes.

Dr. Markus is a member of the American Geophysical Union.



Donald K. Perovich received the M.S. and Ph.D. degrees in geophysics from the University of Washington, Seattle, in 1979 and 1983, respectively.

He is currently a Research Geophysicist with the Snow and Ice Branch, U.S. Army Cold Regions Research and Engineering Laboratory, Hanover, NH. He has conducted wide-ranging studies on sea ice, with special focus on optical properties and radiative transfer in sea ice. He was the Chief Scientist for the SHEBA Project, an experiment where a ship was frozen into the Arctic pack and allowed to drift for a year.

Dr. Perovich is a member of the American Geophysical Union, the International Glaciological Society, the American Meteorological Society, and the Electromagnetics Academy.



John G. Sonntag received the B.S. degree in aerospace engineering from Texas A&M University, College Station, in 1991, and the M.S. degree in aerospace engineering from the University of Texas, Austin, in 1993.

Since 1993, he has been employed by EG&G Technical Services, Inc., Wallops Island, VA, and worked as a member of NASA's Airborne Topographic Mapper project team. He specializes in the application of precise global positioning system technology to airborne remote-sensing problems, and in the applications of airborne LIDAR mapping to polar science.



Julienne C. Stroeve received the B.S. and M.S. degrees in aerospace engineering and the Ph.D. degree in geography from the University of Colorado, Boulder, in 1989, 1991, and 1996, respectively, where she focused on surface energy balance studies of the Greenland ice sheet using satellite imagery.

Since 1996, she has been with the National Snow and Ice Data Center, Cooperative Institute for Research in Environmental Sciences, University of Colorado, Boulder, as a Research Scientist, specializing in remote sensing of snow and ice. She has extensive experience in remote sensing of the polar regions using satellite imagery that spans the optical to the microwave spectral region. She has participated in several field campaigns in Greenland and the Arctic for the purpose of validation of various geophysical parameters retrieved from spacecraft such as sea ice concentration, surface temperature, and surface reflectivity. Additional research projects include monitoring the rapid decline in ice cover in the Arctic and increased melt of the Greenland ice sheet. At NSIDC, she is responsible for the sea ice products derived from satellite passive microwave data, which includes aiding in the design of Web pages providing general sea ice information and data sets regarding the state of sea ice that may be useful to a broad audience.

Dr. Stroeve is a member of the IEEE Geoscience and Remote Sensing Society, the American Geophysical Union, and the Association of American Geographers.



Ken Tape received the M.S. degree in geophysics from the University of Alaska-Fairbanks, Fairbanks, in 2006. He is currently working toward the Ph.D. degree in ecology at the University of Alaska-Fairbanks.

He has participated in numerous winter expeditions on the sea ice and tundra of Northern Alaska.

Mr. Tape is a member of the American Geophysical Union.